Nano Energy 89 (2021) 106447

Contents lists available at ScienceDirect

Nano Energy

journal homepage: www.elsevier.com/locate/nanoen

Full paper

Self-powered strain sensor based on the piezo-transmittance of a mechanical metamaterial

Jimin Gu [a,1], Junseong Ahn [a,b,1], Jiyoung Jung [a], Seokjoo Cho [a], Jungrak Choi [a], Yongrok Jeong [b], Jaeho Park [a], Soonhyoung Hwang [b], Incheol Cho [a], Jiwoo Ko [a,b], Ji-Hwan Ha [a,b], Zhi-Jun Zhao [b], Sohee Jeon [b], Seunghwa Ryu [a], Jun-Ho Jeong [b,*], Inkyu Park [a,*]

[a] Department of Mechanical Engineering, Korea Advanced Institute of Science and Technology (KAIST), Daejeon 34141, Republic of Korea
[b] Department of Nano Manufacturing Technology, Korea Institute of Machinery and Materials (KIMM), Daejeon 34103, Republic of Korea

ARTICLE INFO

Keywords:
Optical strain sensors
Mechanical metamaterials
Auxetic structures
Soft sensors
Self-powered sensors

ABSTRACT

In the field of soft strain sensors, piezo-transmittance based strain sensors, which detect strains by optical transmittance change, have promising advantages of fast response, high sensitivity, long-term stability, and negligible effect from environmental factors. However, they feature low sensor-to-sensor and in-sensor uniformity as well as unpredictable response and high stiffness. This study exploits the gap control of an auxetic-patterned elastomer to develop a piezo-transmittance based strain sensor. Gap opening mechanism in the negative Poisson's ratio metamaterial with rotating square structures makes the sensor free from these limitations; thus, achieving a designable response and low stiffness. In addition, high sensor-to-sensor ((root-mean-square deviation (RSD) < 3.5%) and in-sensor (RSD < 5%) uniformities are achieved by uniform metal-deposited light-blocking film. Finally, the developed sensor has been integrated with a solar cell and Bluetooth Low Energy (BLE) 4.0 to afford a self-powered wireless strain sensing system that is successfully applied to structural health monitoring and human motion monitoring.

1. Introduction

Soft strain sensors, which offer the benefits of high stretchability and mechanical compatibility with curved surfaces, are attracting huge attentions in both soft systems (e.g., human motion monitoring [1–3] (HMM), electronic skins [4–7], healthcare monitoring systems [8,9], and soft robotics [10–12]) and rigid systems (e.g., structural health monitoring (SHM) [13]). Among the soft strain sensors, piezo-resistive and piezo-capacitive sensors have been widely researched [14–16]. However, piezo-resistive devices [17–23] suffer from unstable response and hysteresis, while piezo-capacitive devices suffer from low sensitivity. Moreover, the responses of both types are affected by environmental factors, such as temperature, humidity and electromagnetic interference [24–26]. Therefore, piezo-transmittance based strain sensors, which detect strains based on the changes in the optical transmittance, have garnered attention owing to their advantages such as fast response, high sensitivity, long-term stability, and negligible effect from environmental factors [27,28]. However, the randomness of used nanomaterials (e.g., carbon nanotube (CNT) and TiO_2 nanoparticles) and applicable fabrication methods (e.g., spray coating [27,29–32], mechanical mixing [33,34], and dip coating [35]) result in low in-sensor and sensor-to-sensor uniformities, while the mechanism based on the strain-dependent crack propagation results in unpredictable responses. In addition, current overall soft strain sensors have two common problems. First, even if a soft material such as an elastomer is used as the sensor substrate, the target to be measured is subjected to a mechanical constraint owing to the stiffness of the substrate. Second, previously reported sensors inevitably require a power source for signal detection, whereas self-powered sensor are increasingly required for applications in SHM and wearable devices. Therefore, the development of soft strain sensors that overcome all of these limitations is in high demand but still remains very challenging.

Meanwhile, mechanical metamaterials have attracted attention because of their unique and unprecedented characteristics [36–47]. In particular, auxetic structures feature a negative Poisson's ratio, i.e., expand (rather than contract) in the transverse direction upon stretching

* Corresponding authors.
E-mail addresses: jhjeong@kimm.re.kr (J.-H. Jeong), inkyu@kaist.ac.kr (I. Park).
[1] Jimin Gu and Junseong Ahn contributed equally.

https://doi.org/10.1016/j.nanoen.2021.106447
Received 2 April 2021; Received in revised form 10 July 2021; Accepted 14 August 2021
Available online 19 August 2021

in the longitudinal direction, and this characteristic can significantly affect the sensing performance. Therefore, these structures have been used to improve the performance of piezo-resistive and piezo-capacitive sensors. However, because they only focused on the enhancement of sensitivity, they still have not been able to solve the abovementioned critical problems of soft strain sensors [48–53].

To address the limitations of piezo-transmittance based soft strain sensors associated with the uniformity, response predictability, power consumption, and mechanical stiffness, we developed a self-powered piezo-transmittance based strain sensor using an auxetic structure. It utilizes a uniform Au-deposited elastomer film with a rotating square pattern (GDE-R), and changes its optical transmittance in response to the changes in auxetic pattern gaps under externally applied strains. This gap opening mechanism of GDE-R allows not only a quantitative and rational design of the sensor response using ray-optics simulation but also an ultralow stiffness owing to the bending-dominated deformation. Therefore, we achieved high sensor-to-sensor uniformity (root mean square deviation (RSD) < 3.5%), high in-sensor uniformity (RSD < 5%), response predictability, and low mechanical stiffness during stretching. Additionally, the bending-dominated deformation, not the elongation of material, and the negative Poisson's ratio provide the sensor with high sensitivity (gauge factor (GF) ≈ 10.5), low hysteresis (~0.508%), high linearity (R^2 > 0.997), and long-term stability (>10,000 cycles). For showing the practical applicability and performance demonstration, the developed sensor was integrated into a self-powered wireless strain sensing system (using the response change of a solar cell under natural or artificial light) for SHM and HMM. In the case of SHM, the sensor was used to monitor the inflation and deflation of a soft aerostat and to detect a crack propagation in a rigid structural object. In the case of HMM, our sensor was utilized to implement a real-time monitoring of target muscle contraction and the corresponding joint to prevent injuries caused by incorrect postures during weight training.

2. Results and discussion

2.1. Sensor design and working principle

To develop the optimized predictable and uniform soft piezo-transmittance based sensor, three aspects of the film were considered: the light-blocking material and its fabrication method, the transmittance

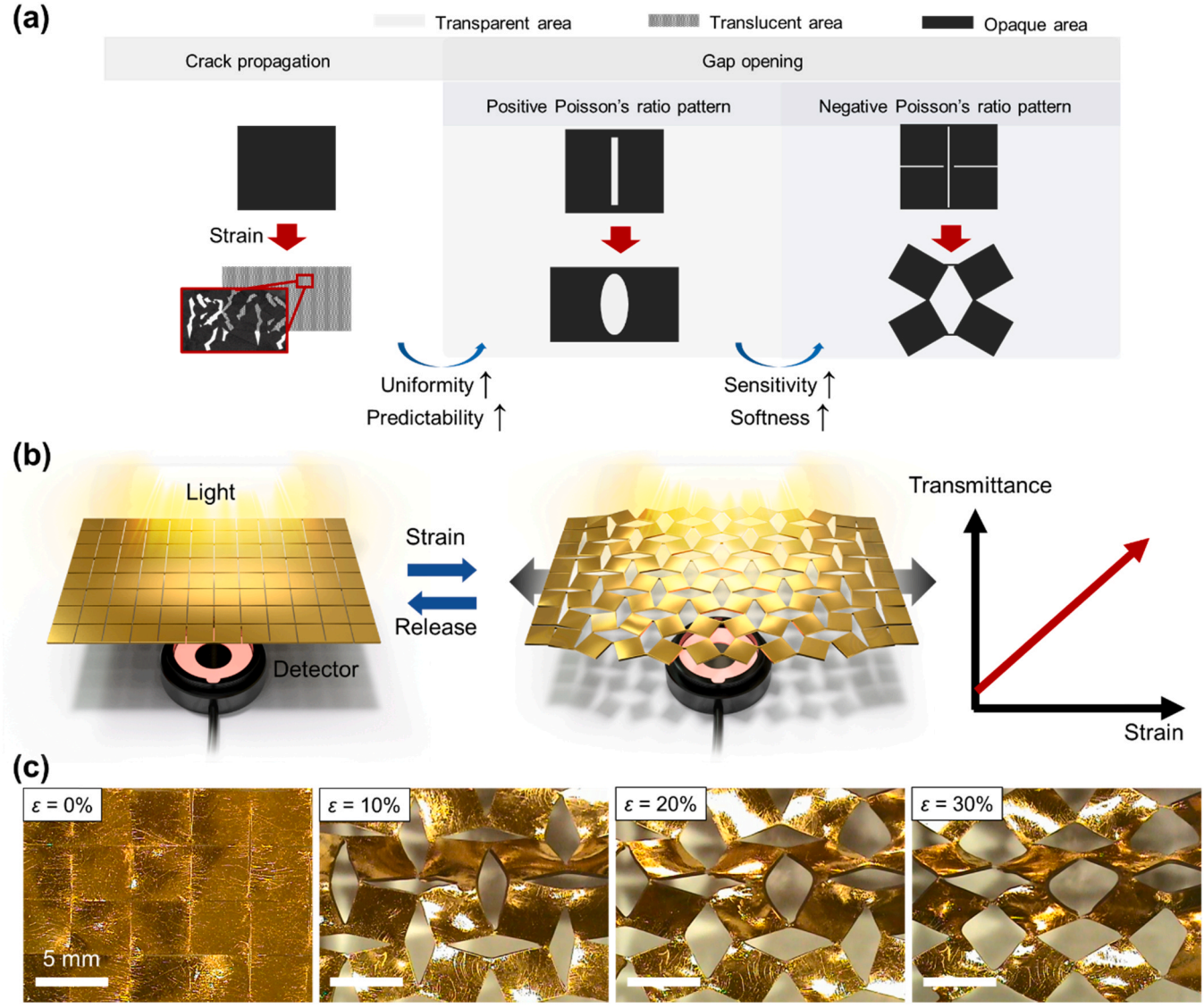

Fig. 1. Design parameters and working principle of the soft piezo-transmittance based strain sensor. a, Schematic of piezo-transmittance mechanisms relying on crack propagation and gap opening with negative/positive Poisson's ratio. b, Schematic representation of the GDE-R based strain sensor. **c**, Images of the GDE-R captured during stretching from $\varepsilon = 0$–30%.

change mechanism, and the sensor structure. First, the light-blocking film and fabrication method affect the uniformity and sensitivity of the piezo-transmittance based strain sensor. In the previous studies, nanomaterials, such as CNT or TiO_2 nanoparticles, were used as the light-blocking materials because of their high optical absorbance in visible range [27,28]. However, the randomness of the materials and fabrication methods inevitably causes low uniformity of sensors. Therefore, in this study, metal thin film using e-beam evaporation is suggested as a light-blocking film owing to its superior uniformity and high reflectance. Second, with regard to the mechanism, the crack propagation and a gap opening are compared for the sensor predictability and uniformity, as shown in Fig. 1(a). Previously reported piezo-transmittance based strain sensors were based on the random crack propagation of the light-blocking material, which makes the sensor response non-predictable and non-designable as well as results in a poor sensor uniformity [27]. Therefore, a novel gap opening mechanism is suggested in this study. Because the gap opening mechanism is based on the predictable deformation of a regular pattern, the sensor response can be rationally designed using numerical simulation. Third, for the sensor structure in this study, gap opening structures with a positive Poisson's ratio and a negative Poisson's ratio were compared for obtaining a high sensitivity and a mechanical softness, as shown in Fig. 1

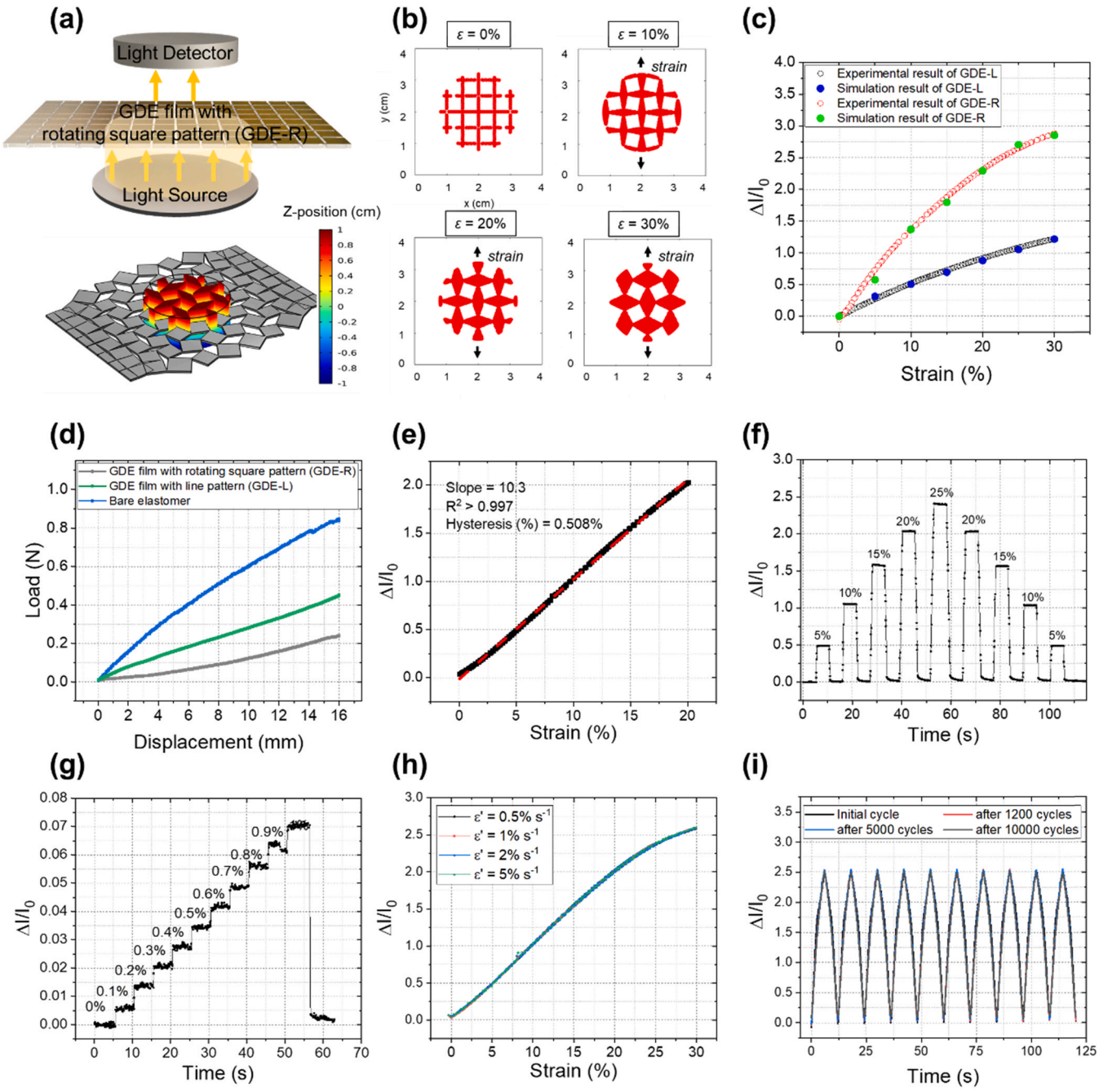

Fig. 2. Results of FEM-based simulation and characterization of the piezo-transmittance based strain sensor based on the GDE-R. a, 3D model used for mechanical and optical simulation, and the result of simulation for 30% strain. b, Light transmitted through the GDE-R (the regions illuminated by the transmitted light are shown in red). c, Comparison of simulated and experimental results obtained for GDE-R and GDE-L. d, Load–displacement curves of bare elastomer, GDE-R, and GDE-L. e, Response to input strain in the range of $\varepsilon = 0$–20%. f, Dynamic responses to static loading. g, Sensor response to small strain inputs (10 × 0.1%). h, Sensor responses at different strain rates. i, Results of a stability test (10,000 cycles) performed in the range of $\varepsilon = 0$–30%.

(a). The structure with a positive Poisson's ratio experiences contraction in the direction perpendicular to that of the applied tensile strain. However, the structure with a negative Poisson's ratio shows an expansion in the direction perpendicular to that of the applied strain, drastically increasing the gap opening in the unit area. In addition, among the negative Poisson's ratio structures, a rotating square pattern exhibits a bending-dominated deformation mode via free rotation of square units in the hinges, leading to an ultralow stiffness [37]. This means that the target object for sensing experiences small load when this structure is utilized as the sensor. Consequently, the GDE-R was selected for the sensor structure owing to its high uniformity, predictability, sensitivity, and mechanical softness.

Fig. 1(b) presents the working principle of the proposed sensor, showing that the light source and the light power detector were positioned on the upper and bottom sides of the GDE-R film, respectively. The transmittance change of the developed GDE-R upon the strain application (i.e., the sensor response) was measured by the light power detector. At zero strain ($\varepsilon = 0\%$), the Au thin film (thickness $t \approx 100$ nm) deposited on the elastomer almost completely blocks the incident light to afford a very low transmission. Upon the application of external longitudinal strain, the amount of light passing through the gaps between the rotating square structures (and thus, the total amount of light transmitted through the GDE-R) increases with progressing hinge rotation. Fig. 1(c) and Video S1 and S2 present a photograph and videos of the GDE-R, revealing that the gaps of the cut pattern increase with increasing external tensile strain. The detailed fabrication process, fabricated image of each sensor, and experimental setups are described in Fig. S1 and S2.

Supplementary material related to this article can be found online at doi:10.1016/j.nanoen.2021.106447.

Supplementary material related to this article can be found online at doi:10.1016/j.nanoen.2021.106447.

2.2. Simulation results and sensor characterization

The sensor response predictability and designability were investigated by mechanical and optical simulations based on the finite element method (FEM), with the 3D modeling and simulation results presented in Fig. 2(a) and (b) and Fig. S3. The GDE-R based sensor and a Au-deposited elastomer film with the line pattern (GDE-L) based sensor were considered, as the fabricated images of each pattern are depicted in Fig. S4. The amount of simulated light transmission was calculated, and compared with the experimental results (marked in red; Fig. 2b and Fig. S5 and S6). Additionally, the solid mechanics results that show Von Mises stress of the GDE-R based sensor are included in Fig. S7. As shown in Fig. 2(c), the simulated and experimental results were in almost perfect agreement with each other, both for GDE-R and GDE-L. As mentioned above, the sensing mechanism of the proposed sensor is based on the predictable behavior of its auxetic structure. Therefore, the sensor response could be easily calculated through numerical simulation, and the results showed that the sensitivity of GDE-R is 2.4 times higher than that of GDE-L. Notably, the slope of the light transmittance change vs. strain plot of GDE-R decreases above applied strain of ~25% as shown in Fig. S8. This behavior is ascribed to the fact that the Poisson's ratio of the employed auxetic pattern remains constant at −1.0 up to a strain of ~30% [40] and then rapidly increases to zero at higher strains.

Next, we analyzed various characteristics of the proposed sensor. Fig. 2(d) and Fig. S9 present the load–displacement curves and photographic image of the bare elastomer, GDE-L and GDE-R with the same dimensions. For a given displacement, the GDE-R based sensor shows 3.53 and 2.39 times lower stiffness than bare elastomer and GDE-L, respectively, due to the rotating square pattern. Fig. S10 presents the load–displacement curves of GDE-R film before breaking, which can endure stretching up to 52 mm (175%) from an initial length of 30 mm. For investigating the sensing performance, given that the sensor response is related to the light transmittance change, we defined GF $= (\Delta I/I_0)/\varepsilon$, where I_0 is the initial light intensity at zero strain, ΔI is the difference between the initial light intensity and the light intensity under applied strain, and ε is the strain. Fig. 2(e) shows that at $\varepsilon = 0$–20%, the sensor features a high GF (10.5), low hysteresis (0.508%), and high linearity ($R^2 > 0.997$). These advantageous characteristics are ascribed to the facts that (i) the employed auxetic structure exhibit a linear area change with increasing applied strain, as discussed in the FEM simulation, and (ii) sensor deformation is mainly caused by the rotation of cut patterns and not by the deformation of the material itself. Fig. 2(f) and Fig. S11 present the dynamic responses of our sensor to various static loading. When a step loading was applied to the sensor, quick response (response time of <20 ms) and recovery were observed during the entire loading-unloading processes. The detailed experiments for calculating the response time of the sensor is described in Fig. S12.

In addition, a strain of 0.1% was applied to the sensor as a step input (Fig. 2g), and the limitofdetection(LOD) $= 3S_b/b$, where S_b is the standard deviation of the y-intercept, and b is the slope of the response in the initial strain range [54], was calculated as 0.01% (Fig. S13). Fig. 2(h) presents the sensor responses at different strain rates ($\varepsilon' = 0.5$–5% s^{-1}), showing that for $\varepsilon = 0$–30%, they are perfectly identical, regardless of the strain rate. In addition, the effect of light source power on the sensor performance was investigated as shown in Fig. S14. The sensor characteristics were independent of the light intensity if the intensity is higher than 29.5 W m^{-2}. Finally, for long-term stability evaluation, the sensor was repeatedly tested for 10,000 cycles in the range of $\varepsilon = 0$–30%. The 10 loading-unloading curves recorded initially and after 1200, 5000, and 10,000 cycles (Fig. 2i) featured identical responses, proving high reliability and repeatability of the sensor.

2.3. Uniformity comparison with a crack propagation-based optical strain sensor

Fig. 3 compares the uniformity of the proposed sensor with that of a previously reported crack propagation-based optical strain sensor comprising a carbon nanotube (CNT)-embedded elastomer (Ecoflex; CEE) composite (Fig. S15). First, sensor-to-sensor uniformities were investigated as shown in Fig. 3(a)–(c). In the CEE-based sensor, the CNT film was deposited by spray-coating, which inhibited the formation of a uniform light-blocking layer. In addition, the crack propagation mechanism hinders the uniform deformation of light-blocking material. Therefore, as can be seen in Fig. 3(a), a large difference in the sensor responses was observed between different CEE-based sensors. On the other hand, the GDE-R based sensor was fabricated using e-beam evaporation and cut in an auxetic pattern to ensure high sensor-to-sensor uniformity (Fig. 3b). Fig. 3(c) shows the RSDs representing the sensor-to-sensor uniformity of CEE and GDE-R based sensors for each strain region. Compared to the CEE-based sensor with an RSD of ~40% at $\varepsilon = 10$–30%, the GDE-R based sensor has much lower RSD (<3.5%) within the same strain region. Second, in-sensor uniformity, reflecting the dependence of sensor response on the in-sensor position (x), was analyzed at $x = -10, -5, 0, 5$, and 10 mm, with $x = 0$ mm indicating the film center. In this experiment, the strain within the film (excluding both ends) can be assumed to be almost constant under an applied uniaxial strain [27]. In the case of the CEE film, the transmittance varies with the locations (Fig. 3d). On the other hand, no significant positional dependence was observed for the GDE-R based sensor, as it featured a uniform Au film and a repetitive pattern (Fig. 3e). Fig. 3(f) shows that the proposed sensor has an RSD (representing in-sensor uniformity) of $\leq 5\%$, and this result is supported by the simulation result in Fig. S16, where the results point out that the sensor response has a position-dependent RSD of $\leq 6.1\%$ due to the effect of pattern size. On the other hand, the CEE-based sensor exhibits a position-dependent RSD of $\leq 30\%$.

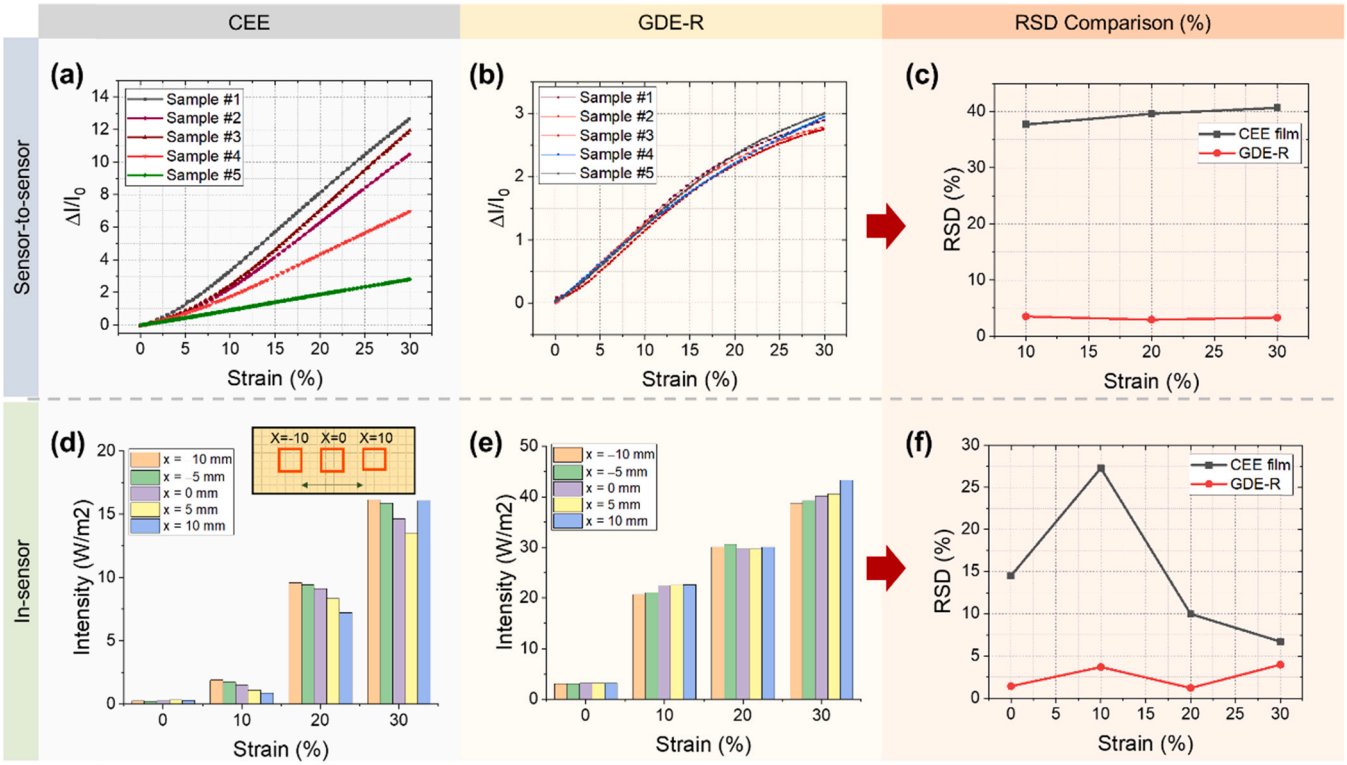

Fig. 3. Uniformity comparison of the piezo-transmittance based strain sensor based on the GDE-R with sensor based on the CEE film. Sensor-to-sensor uniformity in the range of $\varepsilon = 0$–30% determined for five piezo-transmittance based strain sensors based on a, the CEE film and b, the GDE-R. c, Sensor-to-sensor uniformities (RSDs) obtained for the films in a and b. In-sensor uniformity ($x = -10$, -5, 0, 5, and 10 mm) determined at strains of $\varepsilon = 0$–30% for d, the CEE film and e, the GDE-R. f, In-sensor uniformities (RSDs) obtained for the films in d and e.

2.4. Structural health monitoring (SHM) by a self-powered GDE-R based strain sensor

To verify the broad application scopes of the proposed sensor, it was utilized in self-powered SHM and HMM systems. To be suitable for practical applications, the strain sensor should meet the following conditions beyond simply showing good sensing performance. To be suitable for efficient utilization in next-generation wireless Internet of Things (IoT) systems or for the continuous monitoring of target object's strain, the strain sensor should have a low or zero power consumption. Moreover, to ensure that the attachment of the strain sensor does not restrict the target object's motion, the sensor must have lower modulus than the target object. This criterion is particularly important for objects made of soft materials, e.g., air balloons and human skin. Herein, a self-powered sensing system based on solar cell was developed, and the corresponding sensor was shown to have lower modulus than the parent elastomer used in this study due to the auxetic structure. Therefore, the developed sensor is expected to hold great promise for various applications.

Fig. 4(a) shows the developed self-powered wireless strain monitoring system. In this system, a reference solar cell and a sensing solar cell were used to measure the target strain and to calibrate changes in the environmental light. As the current output of the solar cell is proportional to the intensity of the applied light, light calibration could be simplified by a two-point calibration, and the output signal (in arbitrary units) of the Arduino device showed a behavior similar to that conducted in the characterization section (Fig. S17 and S18). The developed sensor was used to monitor the inflation/deflation of an aerostat (Fig. 4b) and the cracks in a rigid specimen (Fig. 4c), which are representative examples of SHM. The detailed experimental setup and the mobile app screen are shown in Fig. S19.

When the developed sensor was attached to the balloon and various strains were applied, the strain measured by the sensor well matched the actual strain (Fig. 4d). In addition, a warning was displayed by the app when the balloon was inflated above the maximum threshold or deflated below the minimum threshold (Fig. 4e and Video S3). Notably, even though the balloon was made of soft materials and had a low stiffness, it could be well inflated when the sensor was attached (Fig. 4f). Fig. 4(g) shows that the developed sensor could well detect the propagation of cracks in a rigid object. Even when the intensity of environmental light was changed, and the signals of the sensing and reference solar cells were varied, the calibrated strain was clearly measured with little disturbance from the environmental light, and cracks were detected (Fig. 4h and Video S4). Furthermore, the change in light was well compensated under the applied strain, as shown in Fig. S20 and Video S5. Fig. 4i demonstrates that even fine strains due to crack propagation can change the unit cell shape of the auxetic structure and thus be detected in solar cells.

Supplementary material related to this article can be found online at doi:10.1016/j.nanoen.2021.106447.

Supplementary material related to this article can be found online at doi:10.1016/j.nanoen.2021.106447.

Supplementary material related to this article can be found online at doi:10.1016/j.nanoen.2021.106447.

2.5. Human motion monitoring (HMM) by a self-powered GDE-R based strain sensor

As a second demonstration, the developed sensor was used for a self-powered HMM during weight training. In general, the repetition of specific postures during weight training aims to stimulate certain target muscles such as the biceps, latissimus dorsi (lats), quadriceps femoris, and pectoralis major. However, despite the availability of correct exercise postures for the target muscles, a risk of injury always exists during

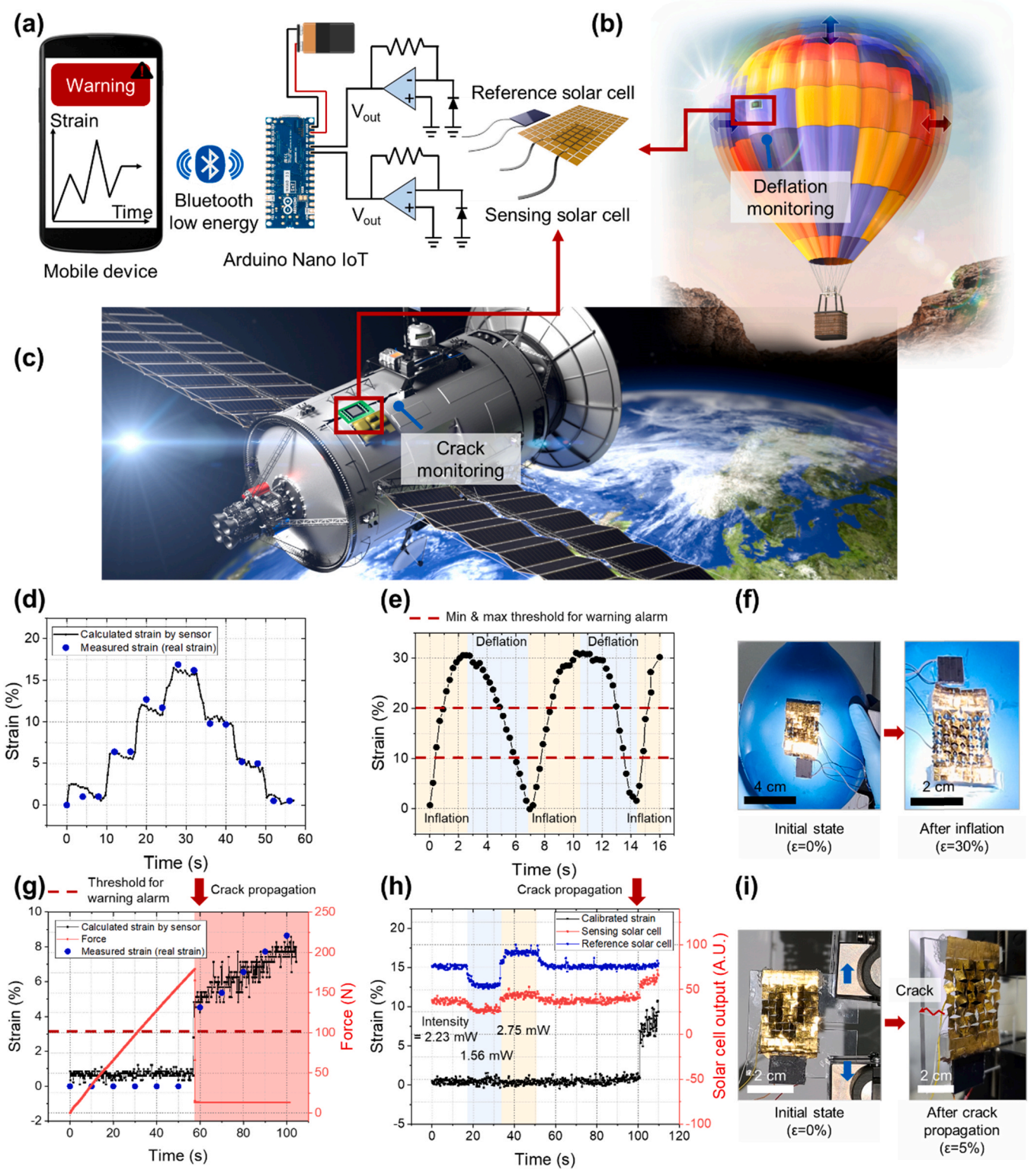

Fig. 4. Application of the developed strain sensor to SHM. a, Schematics of the self-powered wireless monitoring system. Application of the sensor to the monitoring of b, aerostat inflation/deflation and c, crack propagation in an artificial satellite. d, Comparison of real strain with strain measured by the sensor. e, Demonstration of an alarm during balloon inflation/deflation and f, schematics of the experimental setup. g, Experimental result for crack propagation and alarm verification. h, Calibrated strain determined by the reference solar cell and the sensing solar cell at different light intensities. i, Schematics of the experimental setup for crack monitoring.

weight training. The difficulty of quantitatively and accurately monitoring human posture while exercising hinders the prevention of injuries to joints such as the wrist, lower back, and knee, and thus causes serious permanent joint pain [55] Herein, two exercises (arm curl and one-arm dumbbell row) were tested to verify that the developed self-powered wireless sensor is suitable for HMM aimed at posture correction. To simultaneously monitor the correct posture and muscle growth, the sensors were attached to joints with a high risk of injury and the target muscles.

In the case of the arm curl, sensors were attached to the biceps muscle as the target muscle and to the wrist as the injury-prone joint (Fig. 5a). In the case of the one-arm dumbbell row, sensors were attached to the lats as the target muscle and the lower back as the injury-prone joint [55]. When the sensors attached to the wrist and biceps were strained upon motion, the strain measured by individual sensors well matched the real strain (Fig. 5b). Then, the posture of arm curl training was evaluated by the attached sensors. In this case, the strain of the joint part should be lower than the set value, and the strain of the muscle part should be varied during repeated exercise cycles. As shown in Fig. 5 (c)-(i), the strain of each part was clearly measured by the sensors, and the app displayed an alarm when the joint strain exceeded a specific threshold during weight training; the right and wrong postures are shown in Fig. 5(c)-(ii). In addition, the strain changes of individual sensors on the lats and lower back were calibrated and evaluated (Fig. 5d). Similar to the arm curl, sensing accuracy was maintained even in the case of random light changes due to human motion, and the exercise posture of each part could be monitored using the strain change of both sensors (Fig. 5e and Fig. S21). The detailed motions of each posture and the app screen for both exercises are shown in Video S6–S9.

Supplementary material related to this article can be found online at

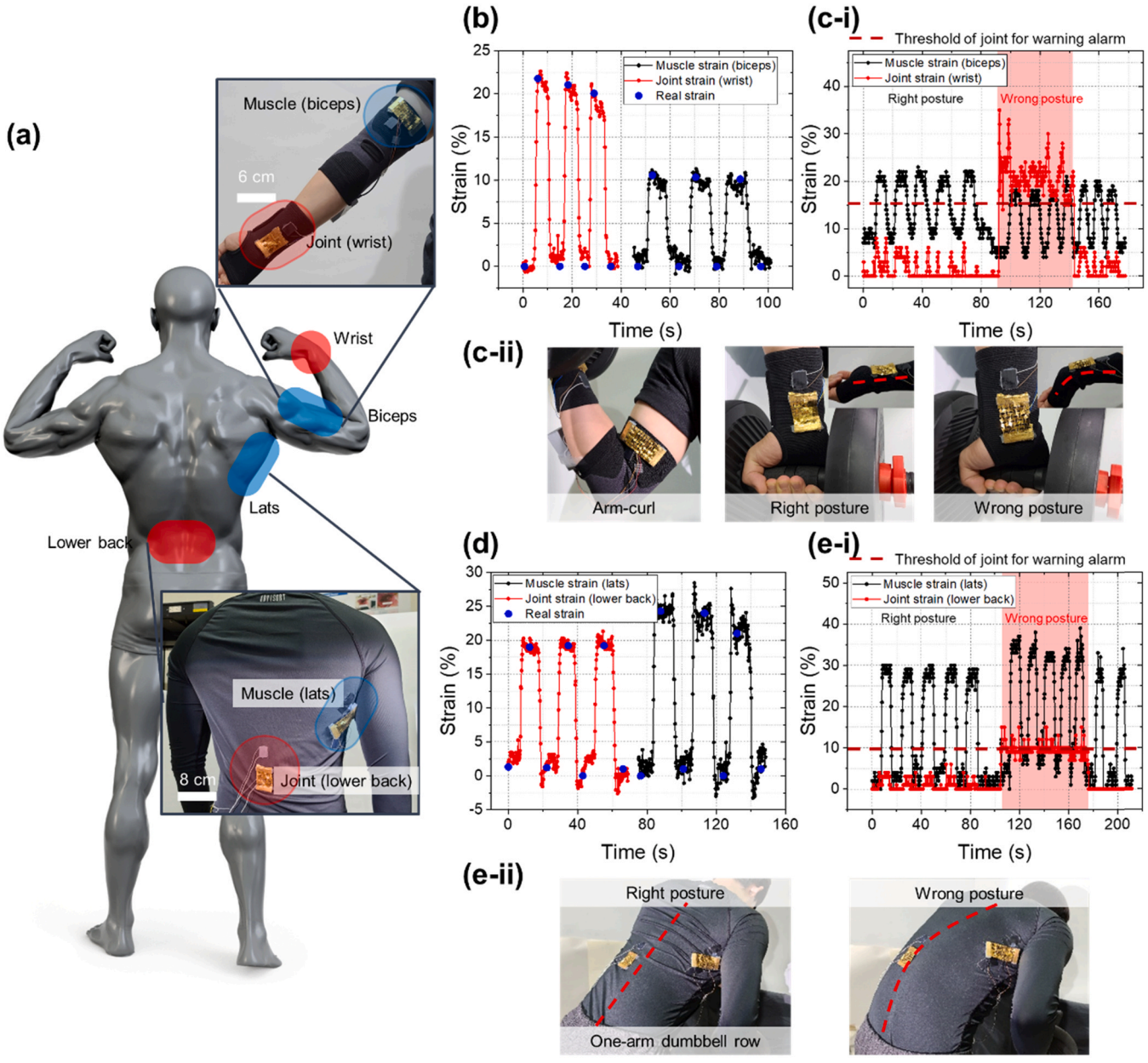

Fig. 5. Application of the developed strain sensor to HMM. a, Schematics and photographic image of integrated strain sensors on the human body. The target muscles and the related joint are indicated with blue and red boxes, respectively. b, Calibrated individual sensor signal for biceps and wrist motion monitoring. c-i, Experimental results and c-ii, photograph for arm curl training with right and wrong postures. d, Calibrated individual sensor signal for the monitoring of latissimus dorsi (lats) and lower back motion. e-i, Experimental results and e-ii, photograph for one-arm dumbbell row training with right and wrong postures.

doi:10.1016/j.nanoen.2021.106447.

Supplementary material related to this article can be found online at doi:10.1016/j.nanoen.2021.106447.

Supplementary material related to this article can be found online at doi:10.1016/j.nanoen.2021.106447.

Supplementary material related to this article can be found online at doi:10.1016/j.nanoen.2021.106447.

3. Conclusion

Herein, we developed a novel strain sensor that overcomes the critical limitations of the soft strain sensors (low uniformity, unpredictable response, high power consumption and high mechanical stiffness) by controlling the gaps in a Au-coated elastomer film with the rotating square pattern (GDE-R). The sensing mechanism of the proposed sensor is based on the optical transmittance change of the GDE-R upon the application of external tensile strain, and the auxetic patterns with uniform light-blocking film realize high sensor-to-sensor uniformity (RSD $<$ 3.5%), high in-sensor uniformity (RSD $<$ 5%), and low mechanical stiffness.

However, three important factors still remain to be considered. First, the auxetic structure used in this study itself does not cause an out-of-plane buckling, but when both edges of the GDE-R are fixed for use as a strain sensor, an out-of-plane buckling occurs under external tensile strain, as shown in Video S1 and S2. It needs to be resolved in subsequent studies because the out-of-plane buckling affects the sensor performance and reduces practical applicability. This phenomenon can be moderated by changing the constraint condition at the edges of the GDE-R such as partial anchoring via properly designed "arms" that help the square units at the edges deform freely [37]. Second, a structural optimization of the GDE-R is required. In this study, only the GDE-R and GDE-L were compared, and the GDE-R showed 2.4 times higher sensitivity than the GDE-L. If the sensor structure is further optimized by designing a rotating square unit of the auxetic structure with the largest gap change by external tensile strain, an improved and optimized sensor can be developed. Third, a completely integrated sensor consisting of a solar cell with piezo-transmittance film needs to be developed. According to the literature, the output signal of a common solar cell is affected by the applied strain [56,57]. Therefore, in this research, we fixed only a small part of the rigid solar cell on the target object using a flexible adhesive to remove the strain effect of the solar cell. However, the final goal of this research is development of a fully integrated system consisting of a solar cell and piezo-transmittance film. Therefore, these issues need to be resolved using a serpentine electrode or stretchable solar cell in our future studies. Therefore, further work is required to reduce the out-of-plane buckling, to optimize the sensor structure, and to implement a fully integrated sensor. Therefore, further work is required to reduce the out-of-plane buckling, optimize the sensor structure, and to implement a fully integrated sensor.

Additionally, the sensitivity (gauge factor, GF) of the piezo-transmittance based strain sensor can be discussed further because it not only depends on the shape of cutting pattern but also on the initial optical transmittance. Because the gauge factor is defined as GF = $(\Delta I/I_0)/\varepsilon$, I_0 can affects the GF. It means that the GF can theoretically increase up to infinity by completely blocking the initial light at zero strain. However, the goal of this research was not only to increase the sensitivity but to also achieve the sensor repeatability and predictability using the auxetic structures. Therefore, we set a reasonably small I0 that can be easily fabricated and controlled by a conventional micro-patterning method (we used plotter in this paper). Even though we did not set a very small I0 for the sensor repeatability, we could accomplish GF of 10.5 by employing auxetic pattern (i.e., by increasing ΔI). To further increase the sensitivity, optimization of the auxetic pattern for increasing ΔI or development of finer patterning method and applying other materials with low transmittance for decreasing I_0 will be studied in a subsequent research.

Despite all these remaining issues, the experimental sensor responses well matched the numerical simulation results and thus indicated the designability and predictability of the proposed sensor. Additionally, our sensor featured high sensitivity (GF $\approx$ 10.5), low hysteresis ($\sim$0.508%), high linearity ($R^2 > 0.997$), and long-term stability. Given that the practical applications of soft strain sensors require low power consumption (to enable integration into IoT systems) and low stiffness (to reduce target object hindrance), we proved the practical applicability of our sensor by integrating it into a self-powered wireless system for SHM and HMM. In the case of SHM, the inflation and deflation of a soft aerostat and the propagation of cracks in a rigid structural object were detected, whereas in the case of HMM, the changes of target muscles and the dorsiflexion of joints at a high risk of injury were monitored. The developed sensor would be suitable for low-power sensing systems and wireless wearable systems linked with emerging application fields in space industry as well as healthcare monitoring systems and industrial IoT systems.

4. Methods

4.1. Film fabrication

The Dragon Skin (DS) 0010 prepolymer (Smooth-On, Inc., USA) base and curing agent were mixed in a 1:1 ratio, and the mixture was spin-coated on a PET film and cured in an oven for 4 h (60 °C). The cured polymer film was detached from the PET film, attached to a cutting mat, and cut with a plotter (CAMEO4; Silhouette America, Inc., USA) to produce an auxetic pattern with a unit cell size of 4 mm. After cutting, the DS film was coated with Cr (thickness $\approx$ 10 nm, deposition rate $\approx$ 1 Å s^{-1}) and Au (thickness $\approx$ 100 nm, deposition rate $\approx$ 1 Å s^{-1}) by e-beam deposition.

4.2. Optical and mechanical simulations

The change of light transmittance upon tensile deformation was simulated using COMSOL Multiphysics software. The GDE-R sensor was placed between the light detector and the light source, and the unit cell and detector sizes were based on the actual experimental setup. The employed model ignored light reflection and diffraction, and assumed a linear elastic material (*Young's modulus (E)* = 300 kPa, Poisson's ratio (ν) = 0.49) and zero gravity. As the solid mechanics condition, to both ends of the film, the prescribed displacement was applied in the x-direction and the constraint was applied in y and z-direction. As the ray optics boundary condition, the film boundary condition was set as the wall condition of "disappear" in COMSOL, which assumes that the light is totally absorbed by the film; in the detection area, the light was set as "freeze" condition in COMSOL, which assumes that the ray stops propagating, to calculate the amount of light that reaches the detector. The solid mechanics simulation results were exported with the deformed shape of the film. The ray optics simulation results were exported into MATLAB to calculate the area of illuminated regions.

4.3. Sensor characterization

A solar illuminator (LAX-C100 Xenon light source, Asahi Spectra Co., Ltd., Inc., Japan) was used as a source of visible light (λ = 400–800 nm), while a power sensor (S120C, Thorlabs, Inc., USA) were used as a light intensity detector (diameter of detecting area = 9.5 mm). The tensile strain was applied by the customized linear stage. The overall scheme of the sensor characterization setup is shown in Fig. S2. The mechanical properties of films were measured using a universal testing machine (AGS-X, Shimadzu, Japan) in the range of displacement = 0–16 mm for 40 mm length samples. Sensor image was taken by using the charge-coupled device (CCD) camera.

4.4. Self-powered wireless sensor system for SHM and HMM

This experiment was approved by institutional review board of KAIST (IRB No. KH2021–004). The self-powered wireless sensing system was constructed using a commercial solar cell (YKSM, YOLK, Republic of Korea) with a size of 20 mm × 16 mm, an Arduino nano33 IoT device, and a mobile phone app designed using MIT App Inventor (App Inventor 2, Google, USA). To eliminate the output signal change of the solar cell with respect to the external strain, we fixed only a small part of the rigid solar cell on the target object using a flexible adhesive. To show the environmental light calibration, we controlled the light intensity by using the solar illuminator (LAX-C100 Xenon light source, Asahi Spectra Co. Ltd. Inc., Japan) power control. The reference solar cell was exposed to the environment light and the sensing solar cell was positioned below the GDE-R film whose light transmittance changed by the external strain. The reference solar cell and sensing solar cell current were increased simultaneously when the environmental light intensity increased; however, only the sensing solar cell current was increased when the GDE-R film was deformed by the external strain. Therefore, for the SHM and HMM demonstrations, output strain was calibrated by the difference between the reference solar cell and sensing solar cell. The current output of the solar cell was converted into a voltage signal by a transimpedance amplifier circuit, and a mobile phone received the signal from the Arduino device using the Bluetooth Low Energy (BLE 4.0) communication protocol. Commercial balloons and customized acrylic specimens were prepared to mimic an aerostat and an artificial satellite system, respectively. During balloon inflation by an air gun and the application of tensile stress to the acrylic specimens using a tensile tester (AGS-X, Shimadzu, Japan), the sensor signal was recorded by a mobile phone. In addition, during the experiment, we fixed only a small part of the rigid solar cell on the target object using a flexible adhesive to eliminate the output signal change of the solar cell with respect to the external strain. A similar system with commercial wrist and elbow protectors was also used for the HMM experiment. The progress of all experiments was recorded by a camera. Videos were captured over a specific period, and the captured images were imported into the CAD program (AutoCAD, Autodesk, USA) to measure real strain.

CRediT authorship contribution statement

Jimin Gu and Junseong Ahn: Conceptualization, Methodology, Visualization. **Jiyoung Jung:** Software. **Seokjoo Cho:** Methodology. **Jungrak Choi:** Visualization. **Yongrok Jeong and Jaeho Park:** Validation **Soonhyoung Hwang:** Writing – original draft. **Incheol Cho:** Validation, Visualization. **Jiwoo Ko:** Methodology. **Ji-Hwan Ha:** Conceptualization. **Zhi-Jun Zhao:** Methodology, Visualization. **Sohee Jeon:** Validation. **Seunghwa Ryu:** Software. **Jun-Ho Jeong:** Supervision. **Inkyu Park:** Supervision.

Declaration of Competing Interest

The authors declare that they have no known competing financial interests or personal relationships that could have appeared to influence the work reported in this paper.

Acknowledgments

This work was supported by the National Research Foundation of Korea (NRF) Grant funded by the Korean Government (MSIP) (No. 2015R1A5A1037668), the National Research Foundation of Korea (NRF) grant funded by the Korea government (MSIT) (No. 2021R1A2C3008742), and the Center for Advanced Meta-Materials (CAMM) funded by the Ministry of Science, ICT and Future Planning, Korea, through the Global Frontier Project (CAMM-No. 2014M3A6B3063707).

Appendix A. Supporting information

Supplementary data associated with this article can be found in the online version at doi:10.1016/j.nanoen.2021.106447.

References

[1] D. Cho, J. Park, J. Kim, T. Kim, J. Kim, I. Park, S. Jeon, Three-dimensional continuous conductive nanostructure for highly sensitive and stretchable strain sensor, ACS Appl. Mater. Interfaces 9 (2017) 17369–17378.
[2] M.S. Kim, K. Kim, D. Kwon, S. Kim, J. Gu, Y.S. Oh, I. Park, Microdome-induced strain localization for biaxial strain decoupling toward stretchable and wearable human motion detection, Langmuir 36 (2020) 8939–8946.
[3] J. Lee, M. Lim, J. Yoon, M.S. Kim, B. Choi, D.M. Kim, D.H. Kim, I. Park, S.J. Choi, Transparent, flexible strain sensor based on a solution-processed carbon nanotube network, ACS Appl. Mater. Interfaces 9 (2017) 26279–26285.
[4] Q. Sun, W. Seung, B.J. Kim, S. Seo, S.-W. Kim, J.H. Cho, Active matrix electronic skin strain sensor based on piezopotential-powered graphene transistors, Adv. Mater. 27 (2015), 3411-7.
[5] J. Ge, L. Sun, F.R. Zhang, Y. Zhang, L.A. Shi, H.Y. Zhao, H.W. Zhu, H.L. Jiang, S. H. Yu, A stretchable electronic fabric artificial skin with pressure-, lateral strain-, and flexion-sensitive properties, Adv. Mater. 28 (2016), 722-8.
[6] S. Xu, D.M. Vogt, W.-H. Hsu, J. Osborne, T. Walsh, J.R. Foster, S.K. Sullivan, V. C. Smith, A.W. Rousing, E.C. Goldfield, R.J. Wood, Biocompatible soft fluidic strain and force sensors for wearable devices, Adv. Funct. Mater. 29 (2019), 1807058.
[7] Y. Wang, S. Lee, T. Yokota, H. Wang, Z. Jiang, J. Wang, M. Koizumi, T. Someya, Structural basis of client specificity in mitochondrial membrane-protein chaperones, Sci. Adv. 6 (2020), eabd0263.
[8] T.Q. Trung, N.-E. Lee, Flexible and stretchable physical sensor integrated platforms for wearable human-activity monitoringand personal healthcare, Adv. Mater. 28 (2016), 4338-72.
[9] S.A. Dual, B. Llerena Zambrano, S. Sündermann, N. Cesarovic, M. Kron, K. Magkoutas, J. Hengsteler, V. Falk, C. Starck, M. Meboldt, J. Vörös, M. Schmid Daners, Continuous heart volume monitoring by fully implantable soft strain sensor, Adv. Healthc. Mater. 9 (2020), 2000855.
[10] K. Elgeneidy, G. Neumann, M. Jackson, N. Lohse, Directly printable flexible strain sensors for bending and contact feedback of soft actuators, Front. Robot. AI 5 (2018) 1.
[11] S. Cheng, Y.S. Narang, C. Yang, Z. Suo, R.D. Howe, Adv. Mater. Interfaces 6 (2019) 1.
[12] V. Sanchez, C.J. Walsh, R.J. Wood, Adv. Funct. Mater. 2008278 (2020) 1.
[13] R. Herbert, H.R. Lim, W.H. Yeo, W.H. Yeo, W.H. Yeo, Printed, soft, nanostructured strain sensors for monitoring of structural health and human physiology, ACS Appl. Mater. Interfaces 12 (2020) 25020–25030.
[14] H. Souri, H. Banerjee, A. Jusufi, N. Radacsi, A.A. Stokes, I. Park, M. Sitti, M. Amjadi, Wearable and stretchable strain sensors: materials, sensing mechanisms, and applications, Adv. Intell. Syst. 2 (2020), 2000039.
[15] T.Q. Trung, N.E. Lee, Flexible and stretchable physical sensor integrated platforms for wearable human-activity monitoringand personal healthcare, Adv. Mater. 28 (2016), 4338-72.
[16] M. Amjadi, K.-U. Kyung, I. Park, M. Sitti, Stretchable, skin-mountable, and wearable strain sensors and their potential applications: a review, Adv. Funct. Mater. 26 (2016) 1678–1698.
[17] S. Wang, K. Chen, M. Wang, H. Li, G. Chen, J. Liu, L. Xu, Y. Jian, C. Meng, X. Zheng, S. Liu, C. Yin, Z. Wang, P. Du, S. Qu, C.W. Leung, Controllable synthesis of nickel nanowires and its application in high sensitivity, stretchable strain sensor for body motion sensing, J. Mater. Chem. C 6 (2018) 4737–4745.
[18] B. Nie, X. Li, J. Shao, X. Li, H. Tian, D. Wang, Q. Zhang, B. Lu, Flexible and transparent strain sensors with embedded multiwalled carbon nanotubes meshes, ACS Appl. Mater. Interfaces 9 (2017) 40681–40689.
[19] J. Ma, P. Wang, H. Chen, S. Bao, W. Chen, H. Lu, Highly sensitive and large-range strain sensor with a self-compensated two-order structure for human motion detection, ACS Appl. Mater. Interfaces 11 (2019) 8527–8536.
[20] Z. Tang, S. Jia, F. Wang, C. Bian, Y. Chen, Y. Wang, B. Li, Highly stretchable core-sheath fibers via wet-spinning for wearable strain sensors, ACS Appl. Mater. Interfaces 10 (2018) 6624–6635.
[21] Y. Zhou, P. Zhan, M. Ren, G. Zheng, K. Dai, L. Mi, C. Liu, C. Shen, Significant stretchability enhancement of a crack-based strain sensor combined with high sensitivity and superior durability for motion monitoring, ACS Appl. Mater. Interfaces 11 (2019) 7405–7414.
[22] Y. Wang, Y. Jia, Y. Zhou, Y. Wang, G. Zheng, K. Dai, C. Liu, C. Shen, Ultra-stretchable, sensitive and durable strain sensors based on polydopamine encapsulated carbon nanotubes/elastic bands, J. Mater. Chem. C 6 (2018) 8160–8170.
[23] S. Zhang, L. Wen, H. Wang, K. Zhu, M. Zhang, Vertical CNT–Ecoflex nanofins for highly linear broad-range-detection wearable strain sensors, J. Mater. Chem. C 6 (2018) 5132–5139.
[24] L. Cai, L. Song, P. Luan, Q. Zhang, N. Zhang, Q. Gao, D. Zhao, X. Zhang, M. Tu, F. Yang, W. Zhou, Q. Fan, J. Luo, W. Zhou, P.M. Ajayan, S. Xie, Super-stretchable, transparent carbon nanotube-based capacitive strain sensors for human motion detection, Sci. Rep. 3 (2013) 3048.
[25] R. Nur, N. Matsuhisa, Z. Jiang, M.O.G. Nayeem, T. Yokota, T. Someya, A highly sensitive capacitive-type strain sensor using wrinkled ultrathin gold films, Nano Lett. 18 (2018) 5610–5617.

[26] H. Xu, Y. Lv, D. Qiu, Y. Zhou, H. Zeng, Y. Chu, An ultra-stretchable, highly sensitive and biocompatible capacitive strain sensor from an ionic nanocomposite for on-skin monitoring, Nanoscale 11 (2019) 1570–1578.
[27] J. Gu, D. Kwon, J. Ahn, I. Park, Wearable strain sensors using light transmittance change of carbon nanotube-embedded elastomers with microcracks, ACS Appl. Mater. Interfaces 12 (2020) 10908–10917.
[28] Q. Zhai, Y. Yang, Highly stretchable variable-transmittance skin for ultrasensitive and wearable strain sensing, Adv. Mater. Technol. 2 (2017), 1700161.
[29] J. Ahn, Y. Jeong, Z.J. Zhao, S. Hwang, K. Kim, J. Ko, S. Jeon, J. Park, H. Kang, J. H. Jeong, I. Park, hot embossing patterning: hot embossing process technology forming arbitrary patterns in real time, Adv. Mater. Technol. 5 (2020), 2070066.
[30] Y. Jeong, J. Park, J. Lee, K. Kim, I. Park, Ultrathin, biocompatible, and flexible pressure sensor with a wide pressure range and its biomedical application, ACS Sens. 5 (2020) 481–489.
[31] J. Ahn, J. Gu, Y. Jeong, K. Kim, J. Jeong, I. Park, Nanotechnology 2019-Janua 2019 303.
[32] Y. Jeong, J. Gu, J. Byun, J. Ahn, J. Byun, K. Kim, J. Park, J. Ko, J. ho Jeong, M. Amjadi, I. Park, Adv. Healthc. Mater. (2021), 2001461.
[33] J. Choi, D. Kwon, K. Kim, J. Park, D. Del Orbe, J. Gu, J. Ahn, I. Cho, Y. Jeong, Y. Oh, I. Park, Synergetic effect of porous elastomer and percolation of carbon nanotube filler toward high performance capacitive pressure sensors, ACS Appl. Mater. Interfaces 12 (2020) 1698–1706.
[34] S. Kim, M. Amjadi, T.I. Lee, Y. Jeong, D. Kwon, M.S. Kim, K. Kim, T.S. Kim, Y.S. Oh, I. Park, Wearable, ultrawide-range, and bending-insensitive pressure sensor based on carbon nanotube network-coated porous elastomer sponges for human interface and healthcare devices, ACS Appl. Mater. Interfaces 11 (2019) 23639–23648.
[35] K. Hwang, J. Ahn, I. Cho, K. Kang, K. Kim, J. Choi, K. Polychronopoulou, I. Park, Microporous elastomer filter coated with metal organic frameworks for improved selectivity and stability of metal oxide gas sensors, ACS Appl. Mater. Interfaces 12 (2020) 13338–13347.
[36] J.N. Grima, K.E. Evans, J. Mater. Sci. Lett. 19 (2000) 1563–1565.
[37] Y. Tang, G. Lin, L. Han, S. Qiu, S. Yang, J. Yin, Design of hierarchically cut hinges for highly stretchable and reconfigurable metamaterials with enhanced strength, Adv. Mater. 27 (2015), 7181-90.
[38] R. Gatt, L. Mizzi, J.I. Azzopardi, K.M. Azzopardi, D. Attard, A. Casha, J. Briffa, J. N. Grima, Specific and common genes implicated across major mental disorders: a review of meta-analysis studies, J. Psychiatr. Res. 60 (2015) 1–13.
[39] A. Lazarus, P.M. Reis, Soft actuation of structured cylinders through auxetic behavior, Adv. Eng. Mater. 17 (2015) 815–820.
[40] Y. Tang, J. Yin, Design of cut unit geometry in hierarchical kirigami-based auxetic metamaterials for high stretchability and compressibility, Extreme Mech. Lett. 12 (2017) 77–85.
[41] H.M.A. Kolken, A.A. Zadpoor, Auxetic mechanical metamaterials, RSC Adv. 7 (2017) 5111–5129.
[42] K. Bertoldi, V. Vitelli, J. Christensen, M. Van Hecke, Nat. Rev. Mater. (2017) 2.
[43] X. Ren, R. Das, P. Tran, T.D. Ngo, Y.M. Xie, Smart Mater. Struct. (2018) 27.
[44] J.U. Surjadi, L. Gao, H. Du, X. Li, X. Xiong, N.X. Fang, Y. Lu, Mechanical metamaterials and their engineering applications, Adv. Eng. Mater. 21 (2019), 1800864.
[45] M.J. Mirzaali, H. Pahlavani, A.A. Zadpoor, Auxeticity and stiffness of random networks: lessons for the rational design of 3D printed mechanical metamaterials, Appl. Phys. Lett. 115 (2019), 021901.
[46] J.K. Wilt, C. Yang, G.X. Gu, Adv. Eng. Mater. (2020) 22.
[47] Z. Wang, C. Luan, G. Liao, J. Liu, X. Yao, J. Fu, The effect of the strain rate on the fretting wear properties of thermally compressed Inconel 625 alloy, Adv. Eng. Mater. 22 (2020), 2070046.
[48] J. Ko, S. Bhullar, Y. Cho, P.C. Lee, M. Byung-Guk Jun, Smart Mater. Struct. (2015) 24.
[49] S.L. Zhang, Y.C. Lai, X. He, R. Liu, Y. Zi, Z.L. Wang, Photovoltaics: deciphering the NH4PbI3 intermediate phase for simultaneous improvement on nucleation and crystal growth of perovskite, Adv. Funct. Mater. 27 (2017), 1770279.
[50] Y. Jiang, Z. Liu, N. Matsuhisa, D. Qi, W.R. Leow, H. Yang, J. Yu, G. Chen, Y. Liu, C. Wan, Z. Liu, X. Chen, Adv. Mater. 30 (2018) 1.
[51] H.W. Kim, T.Y. Kim, H.K. Park, I. You, J. Kwak, J.C. Kim, H. Hwang, H.S. Kim, U. Jeong, Hygroscopic auxetic on-skin sensors for easy-to-handle repeated daily use, ACS Appl. Mater. Interfaces 10 (2018) 40141–40148.
[52] J. Shintake, T. Nagai, K. Ogishima, Sensitivity improvement of highly stretchable capacitive strain sensors by hierarchical auxetic structures, Front. Robot. AI 6 (2019) 1.
[53] J. Wong, A.T. Gong, P.A. Defnet, L. Meabe, B. Beauchamp, R.M. Sweet, H. Sardon, C.L. Cobb, A. Nelson, 3D printing ionogel auxetic frameworks for stretchable sensors, Adv. Mater. Technol. 4 (2019), 1900452.
[54] A. Shrivastava, V. Gupta, Methods for the determination of limit of detection and limit of quantitation of the analytical methods, Chron. Young Sci. 2 (2011) 21.
[55] F. Delavier Strength Training Anatomy, 3rd Edition (Human Kinetics; Third edition, Champaign, 2010).
[56] G. Kim, H. Min, K.S. Lee, D.Y. Lee, S.M. Yoon, S. Il Seok, Impact of strain relaxation on performance of α-formamidinium lead iodide perovskite solar cells, Science 370 (2020) 108–112.
[57] A. Chen, M. Yossef, C. Zhang, Strain effect on the performance of amorphous silicon and perovskite solar cells, Sol. Energy 163 (2018) 243–250.

Jimin Gu is a Ph.D. candidate at the Korea Advanced Institute of Science and Technology (KAIST). She received her M.S. degree at KAIST in 2019. Her current research interest is focused on soft sensors and stretchable electronics for biomedical and healthcare applications.

Junseong Ahn is a Ph.D. candidate at the Korea Advanced Institute of Science and Technology (KAIST). He received his M.S. degree at KAIST in 2019. His current research interest is focused on micro/nano structuring, and their application to sensors/energy harvesting devices.

Jiyoung Jung is a Ph.D. candidate at the Korea Advanced Institute of Science and Technology (KAIST). He received his M.S. degree at KAIST in 2019. His current research interest is focused on composite/device modeling, and their effective behavior.

Seokjoo Cho is an M.S. candidate at the Korea Advanced Institute of Science and Technology (KAIST). He received his B. S. degree at KAIST in 2020. His current research interest is focused on soft sensors and stretchable electronics for biomedical and healthcare applications.

Jungrak Choi is a Ph.D. candidate at the Korea Advanced Institute of Science and Technology (KAIST). He received his M.S. degree at KAIST and DTU in 2018. His current research interest is focused on soft sensors and stretchable electronics for healthcare applications.

Yongrok Jeong is a researcher at the Korea Institute of Machinery & Materials (KIMM). He received his M.S. degree at KAIST in 2018. His current research interest is focused on micro/nano scale structuring and its usage in sensor/actuator systems.

Jaeho Park is a post-doctoral researcher at the Korea Advanced Institute of Science and Technology (KAIST). He received his Ph.D. degree at KAIST in 2019. His current research interest is focused on microscale biosensors and sensor-integrated systems toward biomedical applications.

Soonhyoung Hwang is working as a senior researcher at the Korea Institute of Machinery & Materials (KIMM) in South Korea. He received his doctoral degree from the Department of Materials Science and Engineering of Seoul National University in February 2018. His present research theme involves plasmonic nano-structure fabrication by nanotransfer printing, nanoimprint lithography, E-beam lithography, and KrF lithography. He has experience in the design and fabrication of nano/micro plasmonic optical structures using metals as well as non-metallic materials such as dielectric materials.

Incheol Cho received his B.S. and M.S. degrees from the Department of Mechanical Engineering of the Korea Advanced Institute of Science and Technology (KAIST) in 2015 and 2017, respectively. He is currently a Ph.D. student in the Micro/Nano Transducers (MINT) research group at KAIST. His research interests are low power environmental sensors, nanoscale functional materials, and micro/nano fabrication.

Jiwoo Ko is a Ph.D. candidate at the Korea Advanced Institute of Science and Technology (KAIST). She received her M.S. degree at KAIST in 2018. Her current research interest is focused on nanotransfer printing onto special substrates.

Ji-Hwan Ha is a Ph.D. candidate at the Korea Advanced Institute of Science and Technology (KAIST). He received his M.S. degree at Soongsil University in 2020. His current research interest is focused on electrospun micro/nano composite, and their bio-application.

Zhi-Jun Zhao is a post-doctoral researcher at the Korea Institute of Machinery & Materials (KIMM). He received his Ph.D. degree at Pusan National University in 2018. His research interests are micro-nanofabrication, optical devices, nanomaterial-based sensors, and flexible & wearable electronics.

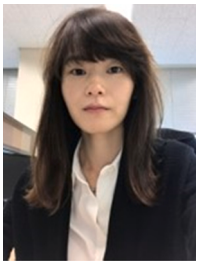

Sohee Jeon is a senior researcher at the Korea Institute of Machinery & Materials (KIMM). She received her Ph.D. degree at Seoul National University in 2014. Her current research interest is focused on nano/micro fabrication toward optoelectronics and biomedical applications.

Seunghwa Ryu received his B.S. and Ph.D. from KAIST (2004) and Stanford (2011), respectively, all in physics. He has been with the Department of Mechanical Engineering at KAIST since 2013 as a faculty member. His research interests include multiscale modeling, homogenization theory, wetting theory, data-driven material/structure design. He has published more than 89 international journal articles. He is a recipient of APACM Award for Young Investigators in Computational Mechanics.

Jun-Ho Jeong is a principal researcher at the Korea Institute of Machinery & Materials (KIMM). He is also a faculty member of the Department of Nano-Mechatronics at the University of Science and Technology (UST). He received his B.S., M.S., and Ph.D. from Hanyang University (1990), Korea Advanced Institute of Science and Technology (KAIST) (1993), and KAIST (1998), respectively, all in mechanical engineering. His research interests are nanoimprinting, nanofabrication, holograms, microneedles, and drug delivery.

Inkyu Park received his B.S., M.S., and Ph.D. from KAIST (1998), UIUC (2003), and UC Berkeley (2007), respectively, all in mechanical engineering. He has been with the Department of Mechanical Engineering at KAIST since 2009 as a faculty member and is currently a KAIST Chair Professor. His research interests include nanofabrication, smart sensors, nanomaterial-based sensors, and flexible & wearable electronics. He has published more than 85 international journal articles (SCI indexed) and 130 international conference proceedings in the area of MEMS/NANO engineering. He is a recipient of the IEEE NANO Best Paper Award (2010) and HP Open Innovation Research Award (2009–2012).